IOP Publishing Journal of Physics: Condensed Matter
J. Phys.: Condens. Matter **29** (2017) 384004 (8pp) https://doi.org/10.1088/1361-648X/aa7cbf

Transparent *p*-CuI/*n*-$BaSnO_{3-\delta}$ heterojunctions with a high rectification ratio

Jeong Hyuk Lee[1], Woong-Jhae Lee[1], Tai Hoon Kim[1], Takhee Lee[2], Seunghun Hong[2] and Kee Hoon Kim[1,2]

[1] Center for Novel States of Complex Materials Research, Department of Physics and Astronomy, Seoul National University, Seoul 08826, Republic of Korea
[2] Institute of Applied Physics, Department of Physics and Astronomy, Seoul National University, Seoul 08826, Republic of Korea

E-mail: khkim@phya.snu.ac.kr

Received 28 March 2017, revised 27 June 2017
Accepted for publication 30 June 2017
Published 21 August 2017

Abstract

Transparent *p*-CuI/*n*-$BaSnO_{3-\delta}$ heterojunction diodes were successfully fabricated by the thermal evaporation of a (1 1 1) oriented γ-phase CuI film on top of an epitaxial $BaSnO_{3-\delta}$(0 0 1) film grown by the pulsed laser deposition. Upon the thickness of the CuI film being increased from 30 to 400 nm, the hole carrier density was systematically reduced from 6.0×10^{19} to 1.0×10^{19} cm^{-3} and the corresponding rectification ratio of the *pn* diode was proportionally enhanced from ~10 to ~10^6. An energy band diagram exhibiting the type-II band alignment is proposed to describe the behavior of the heterojunction diode. A shift of a built-in potential caused by the hole carrier density change in the CuI film is attributed to the thickness-dependent rectification ratio. The best performing *p*-CuI/*n*-$BaSnO_{3-\delta}$ diode exhibited a high current rectification ratio of 6.75×10^5 at ± 2 V and an ideality factor of ~1.5.

Keywords: $BaSnO_3$, copper iodide (CuI), transparent pn diode, high mobility, heterostructure

(Some figures may appear in colour only in the online journal)

1. Introduction

For more than several decades, transparent conducting materials (TCMs), including transparent conducting oxides (TCOs) and transparent oxide semiconductors (TOSs), have been an important class of materials for modern optoelectronic device applications [1, 2]. For example, binary oxides such as ZnO, In_2O_3 and SnO_2 have been used in field-effect transistors (FETs) [3], near UV-emitting diodes [4] and solar cells [5]. However, these well-known materials still have some limitations, particularly in their stability at high temperature and electrical mobility near room temperature [6].

Recently, we found that a new TCO system, i.e. donor doped $BaSnO_3$ with a wide band gap ($E_g = 3.0$–3.1 eV), exhibits high electron mobility up to 320 cm^2 V^{-1} s^{-1} at room temperature and superior thermal stability [7–9]. In order to exploit such unique properties, there currently exists a surge of research efforts to realize $BaSnO_3$-based FETs and *pn* diodes as fundamental building blocks for optoelectronic applications [10, 11]. For the *pn* junctions, *p*-Si/*n*-$Ba_{0.99}La_{0.01}SnO_3$ [12], *p*-(Ba,K)SnO_3/*n*-$Ba_{0.99}La_{0.01}SnO_3$ [13], and *p*-$BaSn_{0.9}Co_{0.1}O_3$/*n*-$BaSn_{0.97}Sb_{0.03}O_3$ have been recently reported [6]. However, those *p*-type (Ba,K)SnO_3 and Ba(Sn,Co)O_3 films have still exhibited very low hole carrier density due to the low activation of carriers (<~10^{15} cm^{-3}) at room temperature [6, 13]. Furthermore, the hole mobility was too small to be measured by conventional Hall effect measurement, presumably because the oxygen *p* orbitals in the top valence band result in a flat band and thus a large hole effective mass [14]. Therefore, it is still necessary to find better performing *p*-type TOSs within the $BaSnO_3$ system or in other material systems.

As parallel efforts, it would be also worthwhile to investigate whether the existing *p*-type TCMs can form a clean *pn*

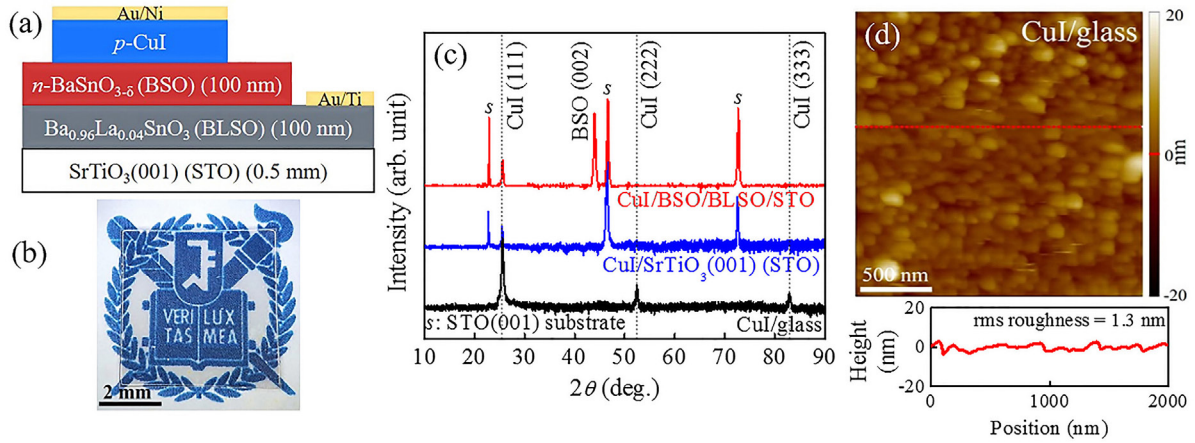

Figure 1. (a) Schematic diagram of the *p*-CuI/*n*-$BaSnO_{3-\delta}$ (BSO) diode grown on a $SrTiO_3$(0 0 1) (STO) substrate (denoted as '*s*' in figure (c)) with a buffer layer of the $Ba_{0.96}La_{0.04}SnO_3$ (BLSO) film. Au/Ni and Au/Ti films were used as an electrode for the CuI and the BLSO films, respectively. (b) A photograph demonstrating the transparency of the CuI/BSO/BLSO/STO(0 0 1) film before deposition of Au electrodes. Thickness of the CuI film in this photograph is 120 nm. (c) X-ray $\theta - 2\theta$ scan results of CuI/BSO/BLSO/STO(0 0 1), CuI/STO(0 0 1) and CuI/glass, all of which exhibit the preferential alignment of the CuI film along (1 1 1) plane. (d) Surface topography of the CuI film grown on the glass substrate. The bottom panel shows a typical height profile along the lateral line drawn in (d).

junction with the donor doped $BaSnO_3$ system. Toward this direction, only a nontransparent *p*-Si/*n*-$Ba_{0.99}La_{0.01}SnO_3$ heterojunction diode has been recently tested [12]. Transparent *pn* diodes, once realized, will obviously be useful for transparent optoelectronic devices. The copper iodide (CuI) in this sense is a promising transparent *p*-type semiconductor with a wide direct band gap ($E_g = 3.1$ eV). Although it was recognized as a *p*-type semiconductor by Baedeker in 1907 [15], it has been recently shown by the Grundmann group that a high quality transparent *p*-CuI/*n*-ZnO heterojunction can be fabricated [16, 17]. Furthermore, various deposition methods have now been established to grow the γ–phase CuI thin films transparently with a high hole carrier density ($>10^{16}$ cm^{-3}) and rather a high hole mobility (~2–25 cm^2 V^{-1} s^{-1}) [17]. Note that the hole mobility of the γ–CuI single crystal reaches as high as 43.9 cm^2 V^{-1} s^{-1} at room temperature, being much higher than those of conventional *p*-type oxides [18, 19]. Because of these advantageous physical properties, CuI has recently been tested in various optoelectronic devices to improve the characteristics of devices such as organic photovoltaics [20], organic light-emitting diodes [21] and solid-state dye solar cells [22].

In this article, we report the successful fabrication of *p*-CuI/*n*-$BaSnO_{3-\delta}$ heterojunction diodes that have exhibited a high rectification ratio of 6.75×10^5 at ± 2 V and an ideality factor of ~1.5. Upon changing the thickness of the CuI film in the diode from 30 to 400 nm, we found that the rectification ratio was systematically enhanced. We propose an energy band diagram for the heterojunction and attribute the rectification ratio increase to the reduction of the built-in potential caused by the hole carrier density decrease.

2. Methods

To prepare targets for thin film deposition, polycrystalline $BaSnO_{3-\delta}$ (BSO) and $Ba_{0.96}La_{0.04}SnO_3$ (BLSO) were synthesized by conventional solid-state reaction methods, starting with high-purity $BaCO_3$, SnO_2 and La_2O_3 powders. Chemicals were weighed in a stoichiometric ratio to form a mixed chemical pellet, which was first calcined at 1250 °C for 6 h and finally sintered at 1450 °C for 24 h after several intermediate grindings. BSO (thickness $t = 100$ nm) and BLSO ($t = 100$ nm) thin films were deposited on $SrTiO_3$(0 0 1) (STO) substrates ($t = 0.5$ mm) via the pulsed laser deposition technique. A KrF excimer laser ($\lambda = 248$ nm) was used at a laser fluence of ~0.6 J cm^{-2} in O_2 pressure of 100 mTorr at 790 °C. Before the deposition of a BSO film, a BLSO film was deposited under the above conditions without further oxygen annealing. Here, the BLSO film is used as a structural buffer layer to reduce threading dislocations coming from the large in-plane lattice mismatch between the STO(0 0 1) substrate and the BSO. At the same time, the BLSO film plays a role of an electrode, exhibiting good ohmic contact with the BSO film. Subsequently, a BSO film was deposited under the same conditions and the as-deposited BSO film was *in situ* annealed at 600 °C for 1 h under O_2 atmosphere with partial pressure of 600 mTorr.

CuI films were deposited by a thermal evaporation method using the high purity CuI powder (~99.998%) at room temperature on the glass (soda-lime glass for a microscope slide, Marienfeld), STO(0 0 1), and BSO/BLSO/STO(0 0 1). In order to make ohmic contacts for the CuI films, Ni ($t = 5$ nm) film was deposited, followed by the deposition of Au ($t = 50$ nm) film as a metallic electrode (denoted as Au/Ni in figure 1(a)). Both CuI and Au/Ni films have been sequentially deposited by the use of stencil masks that allow the fabrication of 5–15 junctions with a lateral dimension of 50×50 μm^2 (square shape) or $\pi \times (50\ \mu m)^2$ (circular shape). The former mask was used in the *pn* junction with the thickness of CuI films (t_{CuI}) from 30–150 nm while the latter was used for one with $t_{CuI} = 400$ nm. In addition, Au ($t = 50$ nm) and Ti ($t = 5$ nm) films (denoted as Au/Ti in figure 1(a)) were deposited by the thermal evaporation to have ohmic contacts for the BSO film. The lateral dimension for Au/Ti electrodes is ~0.2×2 mm^2.

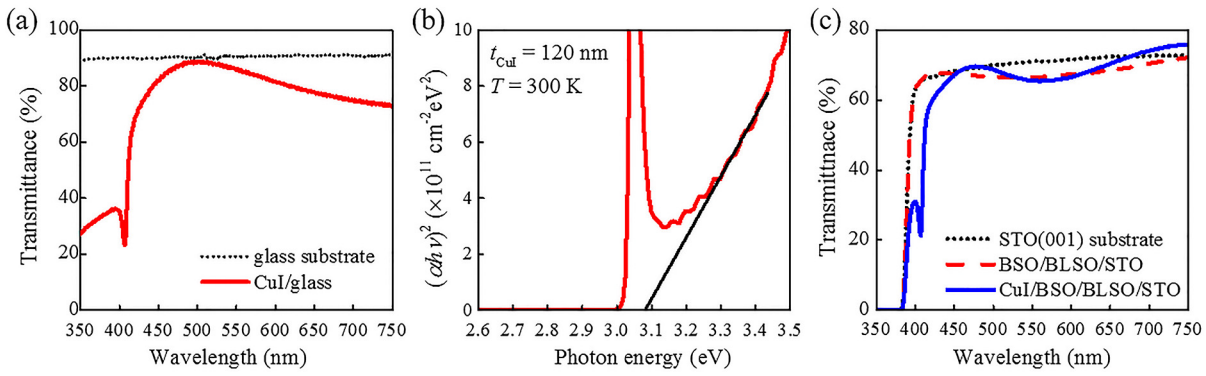

Figure 2. (a) Optical transmittance spectra of the CuI/glass (red solid) and a glass substrate (black dotted) with thickness $t = 1$ mm. (b) The $(\alpha h\nu)^2$ values as a function of photon energy ($h\nu$) for the 120 nm-thick CuI film. Black solid line represents the linear extrapolation to determine an optical band gap of the CuI film. (c) Optical transmittance spectra of the STO(0 0 1) substrate (black dotted) with $t = 0.5$ mm, BSO/BLSO/STO(0 0 1) film (red dashed) and CuI/BSO/BLSO/STO(0 0 1) (blue solid) film. Thickness of each layer is same as that shown in figure 1(a).

We confirmed that both of Au/Ni and Au/Ti electrodes exhibited good ohmic contacts with CuI and BLSO films, respectively.

The crystallinity of the grown films was examined using a high resolution x-ray diffractometer (Empyrean™, PANalytical). The surface morphology was studied using an atomic force microscope (AFM) (NX10™, Park Systems). Optical transmittance measurements of the films were carried out using a UV–VIS–NIR spectrophotometer (Cary 5E™, Varian). The electrical resistivity (ρ), hole carrier density (p) and hole mobility (μ_h) were measured by the Van der Pauw method. Current–voltage (I–V) characteristics were investigated using tungsten probe tips in a semiconductor characterization system (4200-SCS™, Keithley); all the I–V measurements were carried out at room temperature and under ambient atmosphere without exposure to light.

3. Results and discussion

3.1. Structural properties

Figures 1(a) and (b) exhibit a schematic diagram and an actual photograph of the fabricated p-CuI/n-BSO/BLSO/STO(0 0 1) film (before the deposition of Au electrodes), respectively. The p-CuI/n-BSO heterojunction diode was grown on top of the STO(0 0 1) substrate with a BLSO buffer layer ($t = 100$ nm). As demonstrated in figure 1(b), all the fabricated film layers are transparent in visible light. The thicknesses of the p-CuI and n-BSO film in this photograph were 120 nm and 100 nm, respectively.

X-ray $\theta - 2\theta$ scan results of the CuI films grown on BSO/BLSO/STO(0 0 1), STO(0 0 1), and glass substrates are summarized in figure 1(c). The thickness of the CuI films was adjusted to around 120 nm in all the three cases. It turns out that all deposited CuI films exhibit a preferential alignment along the (1 1 1) plane, being consistent with the reported CuI film behavior [17, 19, 23–25]. Because the lattice mismatch between CuI and BSO along the a-axis becomes quite large ~47%, the preferential alignment of the CuI films along (1 1 1) plane is unlikely due to the epitaxial growth mode. In addition, the CuI films grown on the glass substrate also showed similar preferential orientation along the (1 1 1) plane. Moreover, in the growth of the CuI crystal, it was indeed found that the (1 1 1) plane has the highest surface density of atoms as well as the lowest stability energy [26]. Therefore, the preferential alignment of the CuI films can be attributed to the low surface stability energy of the CuI (1 1 1) plane [24].

Figure 1(d) presents the surface topography of the grown CuI films ($t_{CuI} = 120$ nm) on glass substrates as measured by AFM. A root-mean-square (rms) roughness turns out to be ~1.3 nm. The previous thermal evaporation method produced surface roughness of ~2 nm in the films grown on glass substrates [17]. This shows that our CuI films exhibit smooth surface topography which is comparable or slightly superior to the other films grown by the thermal evaporation method [17]. Besides, in our other effort to grow the CuI films by an iodine reaction to the Cu film, we found a much rougher surface of at least 20–30 nm rms roughness because of a large volume expansion occurring during iodization. This observation is consistent with the former studies [16, 17]. Therefore, to form a smooth interface in the p-CuI/n-BSO heterojunction diodes, we employed the thermal evaporation method instead of the iodine reaction method in this work.

3.2. Optical properties

Optical transmittance data of the CuI/glass and a glass substrate in visible light are presented in figure 2(a). An averaged transmittance value of a CuI ($t_{CuI} = 120$ nm)/glass film between 450 and 750 nm is ~80%. Because the CuI film is highly transparent, the reflectivity of the film can be negligible in most of the visible spectral range. In this limit, the absorption coefficient (α) of the CuI film can be approximately estimated from the following equation:

$$\frac{T_{\mathrm{CuI/glass}}}{T_{\mathrm{glass}}} = \mathrm{e}^{-\alpha t_{\mathrm{CuI}}}, \qquad (1)$$

where $T_{\mathrm{CuI/glass}}$ and T_{glass} are the optical transmittance spectra of the CuI/glass and the glass substrate, respectively [27]. In order to determine an optical band gap E_g of the CuI film, the

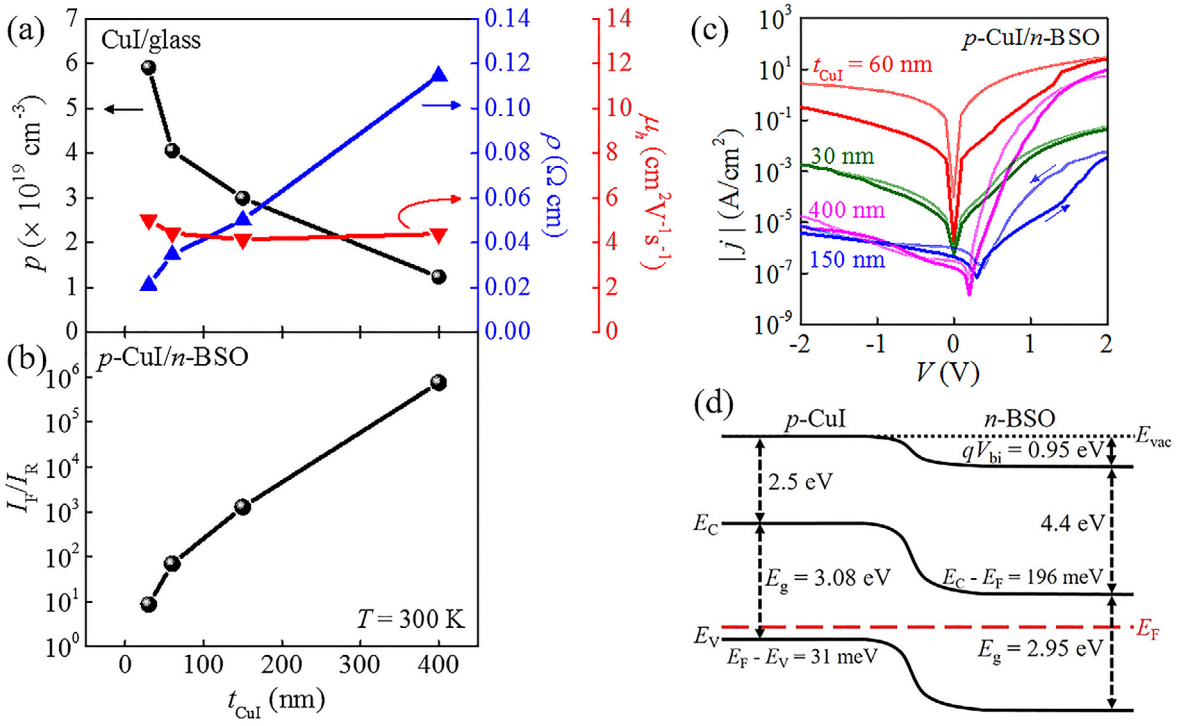

Figure 3. (a) Hole carrier density (p), electrical resistivity (ρ) and hole mobility (μ_h) as a function of thickness of the CuI films (t_{CuI}) grown on glass substrates. (b) The rectification ratio (I_F/I_R) in the p-CuI/n-BSO diodes at various t_{CuI}. (c) The current density–voltage ($|j|$–V) curves of the p-CuI/n-BSO diodes for various t_{CuI}. (d) A proposed energy band diagram of the p-CuI (t_{CuI} = 400 nm)/n-BSO heterojunction diode exhibiting type-II band alignment.

Tauc plot for a direct gap material was constructed from the estimated α, i.e. $(\alpha h\nu)^2$ versus photon energy ($h\nu$) as shown in figure 2(b). A linear extrapolation was used at the absorption edge,

$$(\alpha h\nu)^2 = A\,(h\nu - E_g)\,, \qquad (2)$$

where A is a constant [28]. The optical band gap of the CuI film is found to be ~3.08 ± 0.01 eV, which is indeed consistent with the reported E_g = 3.0–3.1 eV [17, 24]. Besides, a sharp absorption peak observed at 407 nm (~3.05 eV) is due to the well-known interband excitonic transition [25]. The presence of such a sharp excitonic absorption peak supports the high quality of the CuI film.

Furthermore, optical transmittance spectra of the CuI films grown on the glass substrate were also investigated with the variation of t_{CuI} (=20, 30 and 400 nm). Although their averaged transmittance values between 450–750 nm were varied from 65–72%, the optical gap estimated by the Tauc plot were found at an almost similar value of ~3.08 ± 0.01 eV (not shown). In addition, a sharp excitonic absorption peak was observed in all the films investigated with the variation of t_{CuI} = 20–400 nm. These observations indicate that all the CuI films investigated (t_{CuI} = 20–400 nm) have almost the same band structure and high quality of forming an exciton, although their defect levels or effective Fermi level might vary.

Optical transmittance spectra of the STO(0 0 1) substrate, BSO/BLSO/STO(0 0 1), CuI (t_{CuI} = 120 nm)/BSO/BLSO/STO(0 0 1) are compared in figure 2(c). Both transmittance spectra of STO(0 0 1) and BSO/BLSO/STO(0 0 1) maintain high value (~70%) in the visible spectral range. Except for the exciton absorption and the Fabry–Pérot interference, the CuI/BSO/BLSO/STO(0 0 1) film exhibits equally high transparency of ~70%, which is consistent with the fact that the CuI on its own becomes highly transparent (>90%) in most of the visible spectral range [17, 24]. This high transmittance of p-CuI/n-BSO diodes could be useful in future optoelectronic applications requiring high visible transparency.

3.3. Electrical properties

To further understand the electrical properties of CuI films, we have investigated the Hall effect of the CuI films, of which the thickness is systematically varied. Figure 3(a) summarizes the resultant p, ρ and μ_h of the CuI films as a function of t_{CuI}. The Hall coefficient of all the films indeed always exhibited a positive sign, demonstrating that the CuI film is a p-type semiconductor. It is particularly interesting in figure 3(a) to find that the measured p systematically increases as t_{CuI} is decreased. In the CuI system, the Cu vacancy is known to be easily created as a native defect, which should then act as a dominant source of acceptor to result in high p (~10^{19} cm^{-3}) [29]. On the other hand, thermal annealing [19] or thermal evaporation processes [24, 30] have often resulted in iodine deficiency, and as a result, the p-type carrier density has decreased. Therefore, similar to the previous cases [19, 24, 30], a long deposition to fabricate a thick film by thermal evaporation processes might have also created the increase of iodine vacancies. This will naturally lead to the decrease of p as observed in figure 3(a).

Table 1. Input parameters of the Anderson model for the *p*-CuI/*n*-$BaSnO_{3-\delta}$ heterojunction, where m_0 is the electron mass.

Film	Band gap (eV)	Electron affinity (eV)	Carrier density (cm^{-3})	Dielectric constant	Effective mass
p-CuI	3.08	2.5[a]	1.2×10^{19}	15.1[b]	$1.4m_o$[a]
n-$BaSnO_{3-\delta}$	2.95[c]	4.4[d]	2.6×10^{15}[d]	20[e]	$0.35m_o$[f]

[a] Grundmann *et al* [17].
[b] Plendl *et al* [35].
[c] Kim *et al* [8].
[d] Lee *et al* [6].
[e] Singh *et al* [36].
[f] Seo *et al* [37].

As a natural consequence of the decrease of p, ρ of CuI films increases with the increase of t_{CuI} due to the relationship of $\rho = 1/ep\mu_h$, where e is the elementary charge.

Besides, μ_h remained nearly constant or slightly decreases from ~5 to ~4.1 $cm^2\ V^{-1}\ s^{-1}$ with the increase of t_{CuI}. The slight decrease being proportional to t_{CuI} seems to be caused by a major role of ionized impurity scattering (possibly due to Cu vacancy) at this high p regime [17]. However, the μ_h value itself is rather close to, or a bit better than, the typical reported values of thin film mobility in literatures (~2–4 $cm^2\ V^{-1}\ s^{-1}$) at a similar dopant regime but not close to the best reported value of ~25 $cm^2\ V^{-1}\ s^{-1}$ [19, 24]. It is thus likely that our films are subject to other additional scattering from e.g. impurities or grain boundaries.

To investigate further how the change of p can affect the characteristics of the diode, we have fabricated the *p*-CuI/*n*-BSO diodes with the same t_{CuI} variations as in figure 3(a). Figure 3(b) summarizes the current rectification ratios (I_F/I_R) as a function of t_{CuI} in the *p*-CuI/*n*-BSO diodes, where I_F is a current value at +2 V and I_R is a current value at −2 V. Note that the I_F/I_R values varied somewhat among junctions with different areas so that the rectification ratio was determined by having an average in five different diodes for each thickness of the CuI film. However, the stability of the heterojunction, once formed, was quite good; for example, the diode with $t_{CuI} = 400$ nm preserved in a desiccator exhibited almost the same $|j|$–V curve and a similar I_F/I_R value even after ~6 months.

The corresponding typical current density–voltage ($|j|$–V) curves of the *p*-CuI/*n*-BSO diode with variations of t_{CuI} are presented in figure 3(c). In thin CuI films with $t_{CuI} = 30$ or 60 nm, both I_F and I_R are larger than those of thick CuI films with $t_{CuI} = 150$ or 400 nm. This is likely due to the leakage current coming from additional current paths, presumably at the grain boundaries of CuI films. Although our CuI films have a preferential (1 1 1) orientation, it is not epitaxial, presumably due to the random orientation of the in-plane crystal axes across the crystalline domains [23]. Therefore, numerous grain boundaries are expected to exist in the film surface. Such a leakage effect due to the grain boundaries is typically reduced with an increase in film thickness, and such a tendency is consistent with our results in figure 3(c).

What is most interesting in the behavior of the *p*-CuI/*n*-BSO diode is the observation of a systematic increase of I_F/I_R in proportional to t_{CuI} (or inversely proportional to p). In particular, figure 3(c) shows that while the films with $t_{CuI} = 400$ and 150 nm have comparable I_R values, I_F of the film with $t_{CuI} = 400$ nm is much larger than that of $t_{CuI} = 150$ nm, resulting in the enhancement of I_F/I_R from ~10^3 to ~10^6 (figure 3(b)). Such behavior can be understood from variation in the built-in potential (V_{bi}), which generally satisfies the following relationship in a *pn* diode:

$$V_{bi} \propto \ln(N_a), \tag{3}$$

where N_a is the acceptor concentration [31]. An increment of N_a should then increase V_{bi} at the metallurgical junction, reducing the injection of carriers and resulting in the decrease of I_F. The general trend of increasing I_F/I_R in thicker films should be thus associated with the increase of I_F, which is the outcome of the decrease of V_{bi} in the *pn* diode. Collecting all the results in figures 3(b) and (c), we expect that the I_F/I_R value of the *p*-CuI/*n*-BSO diodes could be further improved by minimizing the grain boundaries as well as by reducing p of the CuI film.

Based on the above results in figures 3(a)–(c), an energy band diagram of the *p*-CuI/*n*-BSO heterojunction diode has been constructed in figure 3(d), particularly for the case of $t_{CuI} = 400$ nm. The Anderson model for the heterojunction was used to determine the band alignment [32]; various input parameters of electron affinities [6, 17], dielectric constants [35, 36] and effective masses [17, 37] of both CuI and BSO were adopted from the literatures, while E_g and the carrier concentration of CuI were used from the values determined in this work. Basic parameters and related references are also summarized in table 1.

From the determined parameters in the diode with $t_{CuI} = 400$ nm, the V_{bi}, depletion width for *p*-type material (x_p) and depletion width for *n*-type material (x_n) are predicted as $V_{bi} = 0.95$ V, $x_p = 0.03$ nm and $x_n = 121$ nm, respectively. The estimated depletion widths are indeed consistent with the one-side abrupt diode model [31]. Overall, the resultant band diagram is consistent with the type-II band alignment in the *pn* heterojunction, in which only a conduction band offset of a narrow gap semiconductor is located between the offsets of conduction and valence bands of a wide gap semiconductor [33]. Moreover, the constructed band diagram can qualitatively explain the experimental result in figure 3(b) because the decrease of V_{bi} in proportional to the p value should directly result in the increase of I_F/I_R values.

It is also noted that $x_n = 121$ nm is larger than the thickness of the *n*-type junction itself (~100 nm). In this situation, a finite forward voltage is needed to effectively reduce the

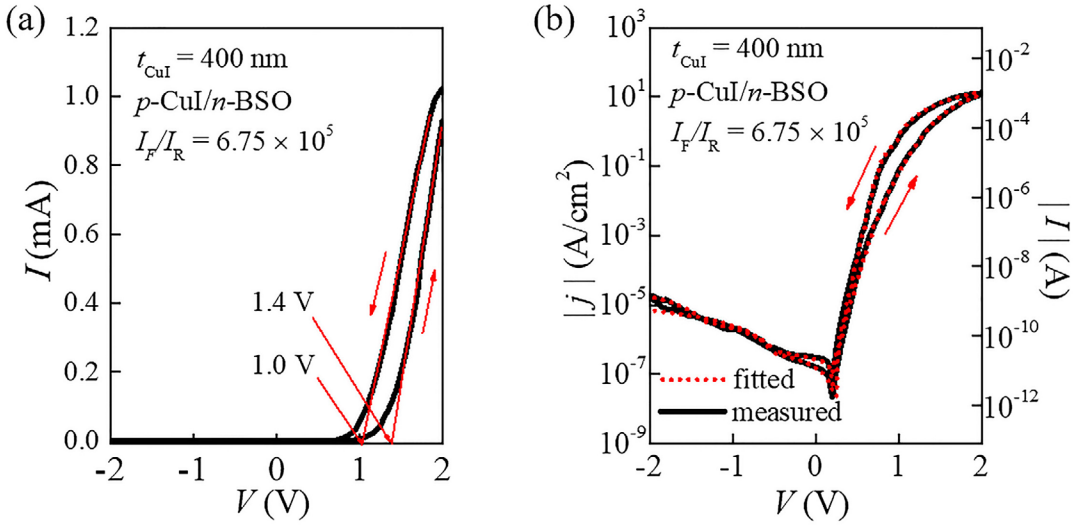

Figure 4. (a) The current–voltage (*I*–*V*) curve of the *p*-CuI ($t_{CuI} = 400$ nm)/*n*-BSO ($t = 100$ nm) diode. Red solid lines represent linear extrapolation to determine the turn-on voltage of the diode. (b) The replotted $|j|$–*V* curve of the same diode from the *I*–*V* curve in (a). The red dotted lines show the fitting curves based on the diode equation (6) and the parameters in table 2.

depletion width and to start the operation of the *pn* diode [13]. Consistent with this scenario, it is indeed found in figure 3(c) that the turning point, at which the sign of current changes from negative to positive, develops at a finite bias voltage; for $t_{CuI} = 400$ and 150 nm, the turning point is located at ~0.2 and ~0.4 V, respectively. Therefore, the observation of the finite value in the turning point can be attributed to the junction thickness being thinner than the depletion width. On the other hand, for the diode with $t_{CuI} = 30$ and 60 nm, a rather large leakage current across the junction seems to erase the finite turning point effect.

Figure 4(a) exhibits the current–voltage (*I*–*V*) curve of the *p*-CuI/*n*-BSO diode with $t_{CuI} = 400$ nm and the turn-on (or knee) voltage as estimated from a linear extrapolation (solid red lines). The turn-on voltage represents an onset of the rapid current increase and is found to be 1.0 V and 1.4 V for reverse and forward bias, respectively. In an ideal situation when the proposed band diagram governs the transport behavior, the turn-on voltage should be directly related to the threshold voltages of electron or hole carriers. In the proposed band diagram, the threshold voltage ($V_{th\text{-}n}$) for the injection of electrons from *n*-BSO to *p*-CuI and the threshold voltage ($V_{th\text{-}p}$) for the transportation of holes from *p*-CuI to *n*-BSO can be estimated from the following equations [34]:

$$V_{th-n} = V_{bi} + \left|\frac{\Delta E_C}{q}\right|, \quad (4)$$

$$V_{th-p} = V_{bi} + \left|\frac{\Delta E_V}{q}\right|, \quad (5)$$

where ΔE_C and ΔE_V are the conduction and valence band offset, respectively. The $V_{th\text{-}n}$ and $V_{th\text{-}p}$ are then calculated to be 2.85 V and 2.77 V, respectively. Thus, the experimental turn-on voltage of ~1.0–1.4 V is obviously smaller than the expected $V_{th\text{-}n}$ and $V_{th\text{-}p}$. Therefore, an actual carrier flow in our device might also be affected by the charge trap state or the interface imperfection, which could provide the additional current path at lower threshold voltages [17]. According to our experimental observation, an applied voltage of $V_a \approx V_{bi}$ seems sufficient to inject electrons (holes) from the *n*-BSO (*p*-CuI) side to the *p*-CuI (*n*-BSO) side [16]. For example, if donor impurity states (effective plus charge state) can be additionally formed due to iodine deficiency inside the bandgap of CuI, electrons are likely to be injected in a forward bias at low threshold voltages.

At least two experimental findings support the presence of many charge trap states at the interface in the fabricated diode. First, there exists significant hysteresis in all the $|j|$–*V* curves in figure 3(c). The hysteresis between the forward and reverse bias curves strongly supports the presence of irreversible charge trapping processes at the interface [16]. Second, the actual saturation current of the diode with $t_{CuI} = 400$ nm (~3.0×10^{-7} A cm^{-2} measured at −0.2 V) exhibited a much larger value than the obtained saturation current (~6.9×10^{-9} A cm^{-2}) from the fitting of the $|j|$–*V* curve (*vide infra*, figure 4(b) and table 2). This difference in the saturation current is usually caused by the interface charge trap [13, 17]. Therefore, the presence of interface charge trap states can explain the discrepancy between expected threshold voltage and the actual turn-on voltage.

Figure 4(b) compares the experimental $|j|$–*V* curve of the *p*-CuI/*n*-BSO diode with $t_{CuI} = 400$ nm, exhibiting the highest rectification ratio, and the fitting curves (dotted red lines) by the diode equation. The $|j|$–*V* curve was fitted by the implicit diode equation of

$$j(V) = j_s\left\{\exp\left[\frac{e(V - IR_s)}{\eta k_B T}\right] - 1\right\} + \frac{V - IR_s}{R_p}, \quad (6)$$

where j_s is the saturation current density, η is the ideality factor, k_B is the Boltzmann constant, T is the absolute temperature, R_s is the series resistance and R_p is the parallel resistance [17]. In table 2, numerical fitting parameters were obtained

Table 2. Numerical fitting parameters were estimated by the diode equation (6) for the $|j|$–V curve of the p-CuI/n-$BaSnO_{3-\delta}$ diode with a 400 nm-thick CuI film.

	Barrier 1 (>0.8 V)			Barrier 2 (<0.8 V)			
Sweeping direction	η	j_S (A cm^{-2})	R_S (Ω)	η	j_S (A cm^{-2})	R_S (Ω)	R_P (Ω)
Forward	2.53	1.44×10^{-9}	456	1.45	1.26×10^{-8}	16976	1.55×10^{9}
Reverse	2.11	6.54×10^{-9}	762	1.59	1.16×10^{-9}	12780	2.49×10^{9}

in two voltage sections for forward and reverse biases based on the assumption of the multi-contacts in the junction [23]. The fitted R_s values from equation (6) are 456 and 762 Ω for forward and reverse bias, respectively. In order to estimate R_s more accurately, R_s has also been determined from the slope of dV/d(ln$I$) ~ 550 Ω [34], which is in agreement with the values obtained from the direct fitting.

It is worthwhile to compare the I_F/I_R of the p-CuI/n-BSO diodes with those of other heterojunction diodes consisting of at least one wide band gap semiconductor; I_F/I_R =3.4 $\times$ 10^2 at $\pm$3 V for p-Si/n-$Ba_{0.99}La_{0.01}SnO_3$ [12], 2 $\times$ 10^7 at $\pm$2 V for p-CuI/n-ZnO (polycrystalline CuI) [17] and 2 $\times$ 10^9 at $\pm$2 V for p-CuI/n-ZnO (epitaxial CuI) [23]. Although the I_F/I_R of the p-CuI/n-BSO diode is still three orders of magnitude smaller than the highest value of I_F/I_R ~ 10^9, the I_F/I_R of the p-CuI/n-BSO diodes have much room for improvement. First, albeit with a large rectification ratio of 6.75 $\times$ 10^5, the R_s value is still rather large in our device. This result comes from the fact that rather a large n-type electrode (~0.4 mm^2) was used as compared with the diode junction area (~0.008 mm^2) [17]. Therefore, if the R_s can be reduced further by the use of a smaller n-type electrode, the I_F/I_R is likely to be enhanced further. Second, a previous report indeed pointed out that p could be further reduced under thermal annealing, which can result in e.g. iodine evaporation to cause further iodine deficiency and Cu vacancy migration into grain boundaries [19]. It is thus highly likely that the rectification ratio of the p-CuI/n-BSO diode can be further improved by thermal annealing as well as electrode size control.

4. Conclusions

We have investigated the electrical properties of transparent p-CuI/n-$BaSnO_{3-\delta}$ heterojunction diodes, for which thermal evaporation and pulsed laser deposition methods have been employed to grow (1 1 1) oriented CuI and epitaxial $BaSnO_{3-\delta}$(0 0 1) films, respectively. Upon increasing the thickness of the CuI film in the diode, we have found a systematic decrease in hole carrier density and an increase to the rectification ratio I_F/I_R, which can be successfully explained by the decrease to a built-in potential in the heterojunction with the type-II band alignment. We have obtained the I_F/I_R = 6.75 $\times$ 10^5 and an ideality factor η = ~1.5 in the best-performing specimen. The present p-CuI/n-$BaSnO_{3-\delta}$ diode can be applicable as current rectifying components in transparent optoelectronic devices.

Acknowledgments

This work was financially supported by the National Creative Research Initiative (2010-0018300) and the Korea–Taiwan Cooperation Program (0409-20150111) through the NRF of Korea funded by the Ministry of Education, Science and Technology. This work was also supported by the Korea Institute of Energy Technology Evaluation and Planning funded by the Ministry of Trade, Industry & Energy of the Republic of Korea (20173010012940). TL thanks the support from the National Creative Research Initiative (2012026372). SH acknowledges the support from the NRF grant (H-GUARD 2013M3A6B2078961).

References

[1] Ginley D S and Bright C 2000 *MRS Bull.* **25** 15
[2] Yu X, Marks T J and Facchetti A 2016 *Nat. Mater.* **15** 383
[3] Hoffmann R C, Kaloumenos M, Heinschke S, Erdem E, Jakes P, Eichel R-A and Schneider J J 2013 *J. Mater. Chem.* C **1** 2577
[4] Hosono H, Ohta H, Hayashi K, Orita M and Hirano M 2002 *J. Cryst. Growth* **237** 496
[5] Calnan S and Tiwari A N 2010 *Thin Solid Films* **518** 1839
[6] Lee W-J, Kim H J, Kang J, Jang D H, Kim T H, Lee J H and Kim K H 2017 *Annu. Rev. Mater. Res.* **47** 391–423
[7] Kim H J *et al* 2012 *Appl. Phys. Express* **5** 061102
[8] Kim H J *et al* 2012 *Phys. Rev.* B **86** 165205
[9] Lee W-J, Kim H J, Sohn E, Kim H M, Kim T H, Char K, Kim J H and Kim K H 2015 *Phys. Status Solidi* a **212** 1487
[10] Kim U, Park C, Ha T, Kim Y M, Kim N, Ju C, Park J, Yu J, Kim J H and Char K 2015 *APL Mater.* **3** 036101
[11] Fujiwara K, Nishihara K, Shiogai J and Tsukazaki A 2016 *AIP Adv.* **6** 085014
[12] Luo B C, Wang J, Cao X S and Jin K X 2014 *Phys. Status Solidi* a **211** 705
[13] Kim H M, Kim U, Park C, Kwon H and Char K 2016 *APL Mater.* **4** 056105
[14] Wang Z, Nayak P K, Caraveo-Frescas J A and Alshareef H N 2016 *Adv. Mater.* **28** 3831
[15] Baebeker K 1907 *Ann. Phys.* **327** 749
[16] Schein F-L, von Wenckstern H and Grundmann M 2013 *Appl. Phys. Lett.* **102** 092109
[17] Grundmann M, Schein F L, Lorenz M, Bontgen T, Lenzner J and von Wenckstern H 2013 *Phys. Status Solidi* a **210** 1671
[18] Chen D, Wang Y, Lin Z, Huang J, Chen X, Pan D and Huang F 2010 *Cryst. Growth Des.* **10** 2057
[19] Yamada N, Ino R and Ninomiya Y 2016 *Chem. Mater.* **28** 4971
[20] Das S, Choi J-Y and Alford T L 2015 *Sol. Energy Mater. Sol. Cells* **133** 255
[21] Lee J-H, Leem D-S and Kim J-J 2008 *Org. Electron.* **9** 805

[22] Cheng C H, Wang J, Du G T, Shi S H, Du Z J, Fan Z Q, Bian J M and Wang M S 2010 *Appl. Phys. Lett.* **97** 083305
[23] Yang C, Kneiss M, Schein F L, Lorenz M and Grundmann M 2016 *Sci. Rep.* **6** 21937
[24] Zi M, Li J, Zhang Z, Wang X, Han J, Yang X, Qiu Z, Gong H, Ji Z and Cao B 2015 *Phys. Status Solidi* a **212** 1466
[25] Kim D, Nakayama M, Kojima O, Tanaka I, Ichida H, Nakanishi T and Nishimura H 1999 *Phys. Rev.* B **60** 13879
[26] Li W J and Shi E W 2002 *Cryst. Res. Technol.* **37** 1041
[27] Pankove J I 1975 *Optical Processes in Semiconductors* (New York: Dover) pp 87–95
[28] Tauc J, Grigorovici R and Vancu A 1966 *Phys. Status Solidi* b **15** 627
[29] Wang J, Li J and Li S-S 2011 *J. Appl. Phys.* **110** 054907
[30] Lin G, Zhao F, Zhao Y, Zhang D, Yang L, Xue X, Wang X, Qu C, Li Q and Zhang L 2016 *Materials* **9** 990
[31] Sze S and Lee M-K 2012 *Semiconductor Devices* (New York: Wiley) pp 82–120
[32] Chuang S L 1995 *Phys. Optoelectron. Devices* (New York: Wiley) pp 21–80
[33] Neamen D A 2003 *Semiconductor Physics and Devices: basic Principles* (Boston, MA: McGraw-Hill) pp 349–54
[34] Javaid K, Xie Y F, Luo H, Wang M, Zhang H L, Gao J H, Zhuge F, Liang L Y and Cao H T 2016 *Appl. Phys. Lett.* **109** 123507
[35] Plendl J N, Hadni A, Claudel J, Henninger Y, Morlot G, Strimer P and Mansur L C 1966 *Appl. Opt.* **5** 397
[36] Singh P, Brandenburg B J, Sebastian C P, Singh P, Singh S, Kumar D and Parkash O 2008 *Japan. J. Appl. Phys.* **47** 3540
[37] Seo D, Yu K, Chang Y J, Sohn E, Kim K H and Choi E J 2014 *Appl. Phys. Lett.* **104** 022102